Crystallization and Melting Behavior of Poly(ϵ-caprolactone) under Physical Confinement

Rong-Ming Ho* and Yeo-Wan Chiang

Department of Chemical Engineering, National Tsing Hua University, Hsinchu 30013, Taiwan, R.O.C.

Chu-Chien Lin and Bor-Han Huang

Department of Chemistry, National Chung-Hsing University, Taichung 40227, Taiwan, R.O.C.

Received December 2, 2004; Revised Manuscript Received March 29, 2005

ABSTRACT: The crystallization and melting behavior of poly(ϵ-caprolactone) (PCL) in a physically confined system, self-assembly blends of poly(ϵ-caprolactone)/polystyrene-*b*-poly(ethylenepropylene) (PCL/PS−PEP), were studied by differential scanning calorimetry (DSC). The glassy PS-rich phases effectively confine the PCL crystallization due to the localization behavior of PCL where the PCL component appears to be localized in between the lamellae-like microdomains of PS block. Macrophase-separated and microphase-separated morphology were both identified in the self-assembly blends. The crystallization rate of PCL is strongly affected by the phase-separated morphology. The effective confinement on crystallization occurs while the size of lamellae-like confinement goes below submicrometer. Under effective confinement, the crystalline chains of PCL appear in random orientation at low crystallization temperature and in parallel orientation at high crystallization temperature as evidenced by simultaneous small-angle X-ray scattering and wide-angle X-ray diffraction experiments. Furthermore, the PCL crystals form multilayer-like crystalline morphology under confinement as evidenced by transmission electron microscopy. On the basis of Avrami treatment, the crystallization kinetics of PCL in a physically confined system and of PCL homopolymer were both studied for comparison. Similar to the PCL homopolymers, the crystallization of localized PCL chains under confinement exhibits a heterogeneous nucleation process. Recognizable melting depression was identified for PCL under confinement whereas significant decrease on relative crystallinity was observed for PCL chains crystallized at higher temperature. As a result, the changes of the crystallization and melting behavior are indeed attributed to the effect of confinement that is strongly dependent upon the spatial size of confinement. Contrary to typical microphase-separated morphology of crystallizable block copolymers (designated as chemically confined system for crystallizing blocks), the unique phase-separated morphology as a physically confined system for the crystallization of PCL provides a representative system for understanding the behavior of crystallization under spatial confinement from tens of nanometers to submicrometers.

Introduction

Crystallization behavior under nanoscale spatial confinement has drawn extensive studies in recent years due to the prerequisite for the basic understanding of crystallization in the applications of nanotechnologies.[1] Different approaches have been carried out in order to explore the effects of confinement on crystallization.[2−34] In particular, the crystallization behavior of semicrystalline block copolymers, in which at least one of the constituted blocks is crystallizable, has been thoroughly studied. The incorporation of crystallizable segments within block copolymers might effectively raise the service temperature and reinforce the mechanical properties of the block copolymers as well as add the complexities of microphase-separated morphology. The kinds of confined environments have been classified into three different circumstances such as one-dimensional, two-dimensional, and three-dimensional confinements according to microphase-separated nanostructural geometries (i.e., lamellae, cylinders, and spheres in sequence), frustrating the crystal growth therein.[35] Systematic studies with respect to the crystallization in these various microstructures have been carried out, and it is evident that the final morphology is found to be strongly dependent upon the experimental temperature, with respect to the order−disorder transition temperature (T_{ODT}), the crystallization temperature of the crystallizing block (T_c^c), the glass transition of the amorphous block (T_g^a), and the crystallization rate. In other words, the final morphology is the consequence of microphase separation, crystallization, and vitrification.[2−6]

To be specific, when $T_c^c > T_{ODT} > T_g^a$, it is generally agreed that the final morphology is driven by crystallization regardless of microphase separation.[3−6] For system with $T_{ODT} > T_g^a > T_c^c$ (this is a hard confinement for crystallization),[7−22] the ordered microstructure can be persevered due to the vitrified microdomains of amorphous blocks. In contrast, if $T_{ODT} > T_c^c \geq T_g^a$, the effect of crystallization on the morphological changes becomes more complicated (this is a soft confinement).[23−34] As suggested by Register and co-workers, the final morphology of crystallized block copolymers resulting from the competition between crystallization and microphase separation can be justified in accordance with the ratio of segregation strength of microphase separation at T_c and at T_{ODT} (i.e., $(\chi N_t)_c$/

* To whom correspondence should be addressed: Tel 886-3-5738349; Fax 886-3-5715408; e-mail rmho@mx.nthu.edu.tw.

10.1021/ma047515l CCC: $30.25
Published on Web 05/03/2005

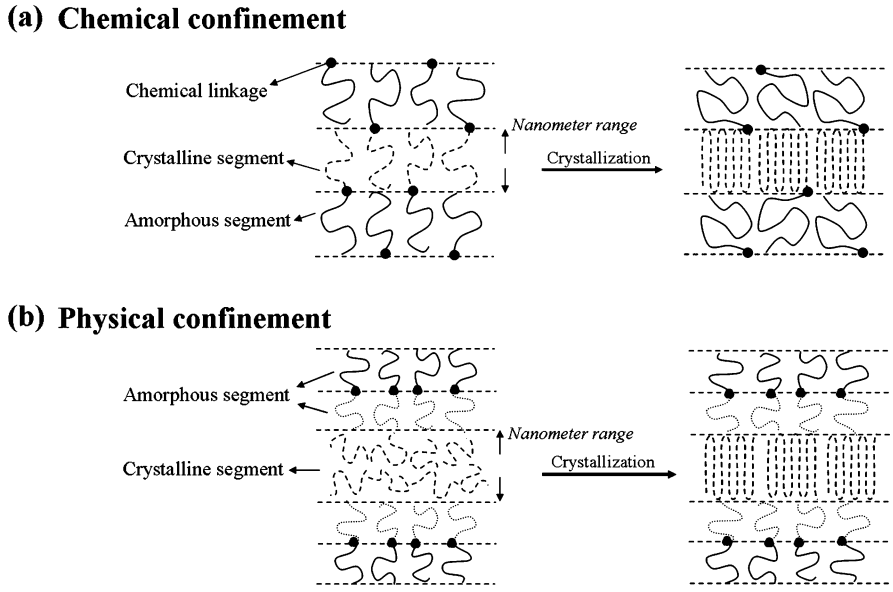

Figure 1. Schematic pictures of (a) chemical confinement and (b) physical confinement.

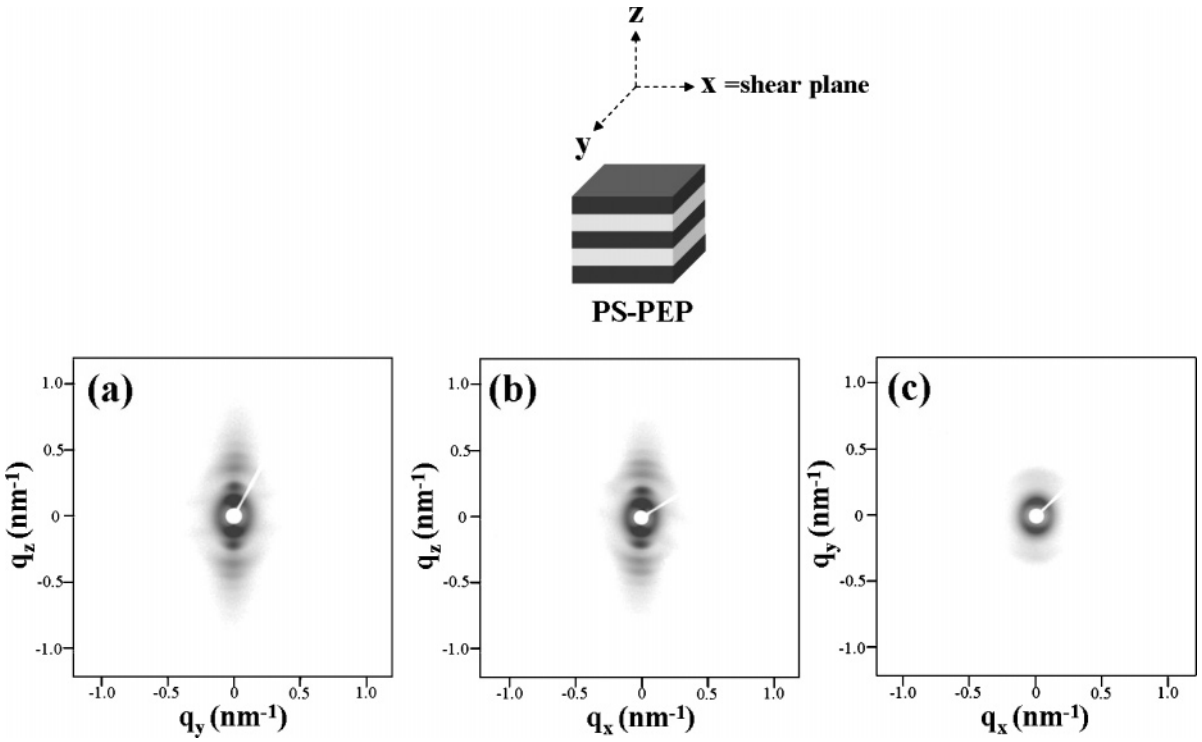

Figure 2. 2D SAXS of orientated neat PS−PEP obtained when X-ray beam is along (a) *x*-direction, (b) *y*-direction, and (c) *z*-direction.

$(\chi N_t)_{ODT}$).[32,33] In principle, the large value of $(\chi N_t)_o/(\chi N_t)_{ODT}$ ratio will lead to the formation of confined morphology for crystallization whereas the small value of $(\chi N_t)_o/(\chi N_t)_{ODT}$ ratio will result in the breakout of microphase-separated morphology.

For crystallizable block copolymers, the confinement is attributed to the formation of preexisting microdomains driven by the incompatibility between the constituted blocks that are chemically linked together at their ends by copolymerization. Recently, a unique morphology possessing a crystallizable PCL component localized favorably within PS-rich constituted lamellar in a PS−PEP block copolymer has been obtained in our laboratory.[36] Contrary to the chemical confinement as illustrated in Figure 1a, self-assembly-induced compatibilization gives rise to the semicrystalline homopolymer localizing in one-block microdomain and consequently creates a specific environment for crystallization where the crystallizing chains are free from the constrain of chemical connection (see Figure 1b). As a result, we named the assembly microstructure as physically confined system for crystalline polymer being distinct from the chemically confined system. Furthermore, macrophase-separated and microphase-separated morphologies having PCL domain sizes above and below submicrometer, respectively, can be simply obtained by blending various PCL homopolymers with PS−PEP block copolymer. It will be interesting to examine the effect of confined size ranging from tens of nanometers up to submicrometers on polymer crystallization.

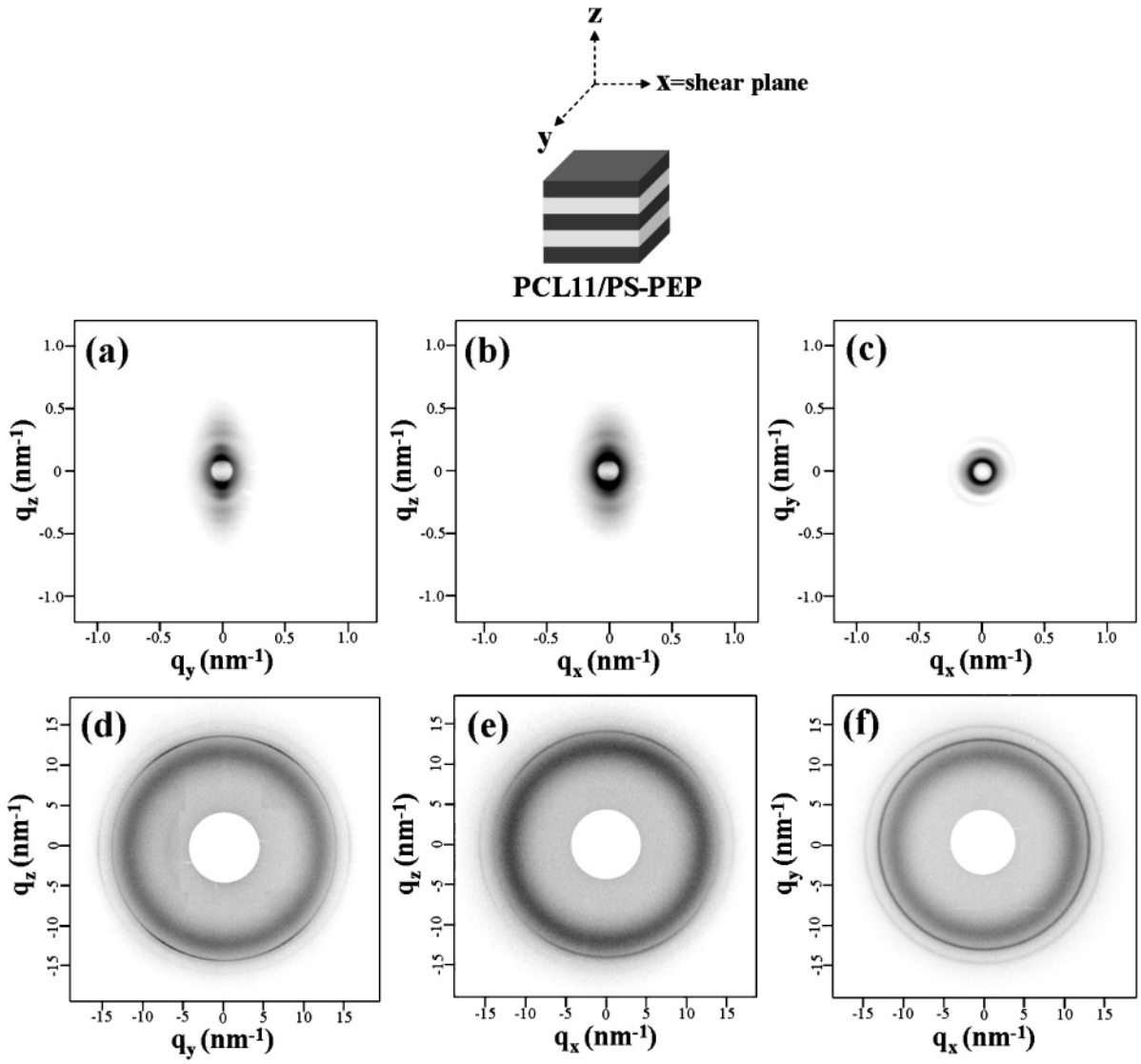

Figure 3. Simultaneous SAXS and WAXD patterns of orientated PCL11/PS−PEP samples isothermally crystallized at 40 °C from ordered melt at 100 °C. 2D SAXS (above) and 2D WAXD (below) obtained (a) along *x*-direction, (b) along *y*-direction, and (c) along *z*-direction.

Experimental Section

Materials. The styrenic triblock copolymer used in this investigation was a diblock copolymer of polystyrene-*b*-poly(ethylenepropylene) symbolized as PS−PEP (Kraton G1701 of Shell Co.). According to the supplier, this commercial PS−PEP contains 37 wt % styrene content. Size exclusion chromatography (SEC) indicated that the number-average molecular weight, M_n, of as-supplied PS−PEP is ca. 211 000 g/mol with a polydispersity index of ca. 1.12. Various poly(ϵ-caprolactone) (PCL) samples with narrow polydispersity index were synthesized in terms of living and immortal polymerization of lactones catalyzed by a novel aluminum alkoxide. The detailed synthetic routes and the sample code of the PCL homopolymers (see Table 1 of ref 36) were described in our previous papers.[36]

Blending Processes. PCL/PS−PEP blends were prepared by melt-mixing in a MiniMax mixer. The MiniMax mixing cup was preheated to 250 °C, and 0.15 g of the PCL[37] powder and 0.85 g of PS−PEP powder were simultaneously introduced. Each blend was melt processed at 250 °C for 10 min at 400 rpm. The detailed mixing procedure was described in our previous paper.[36] After processing, the samples were quenched by ice water. Therefore, well-oriented samples can be obtained by melt-mixing process. The film thickness of PCL/PS−PEP blends is 1 mm. Shear (velocity), vorticity, and velocity gradient directions were assigned as *x*, *y*, and *z* direction, respectively.

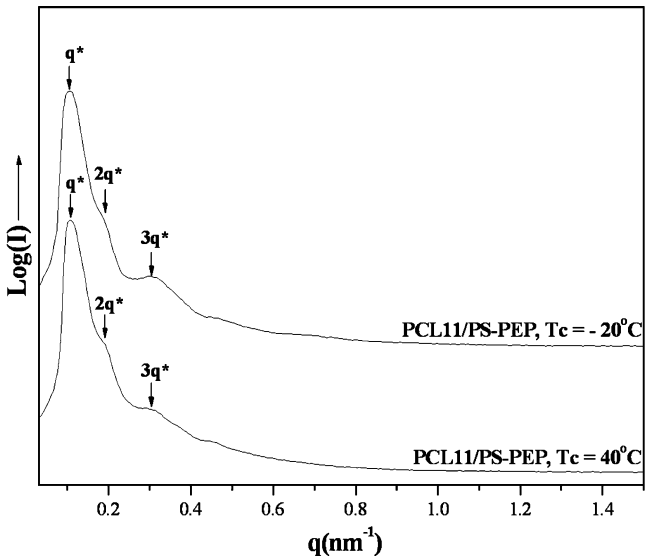

Figure 4. 1D SAXS profiles of PCL11/PS−PEP at $T_c = -20$ and 40 °C.

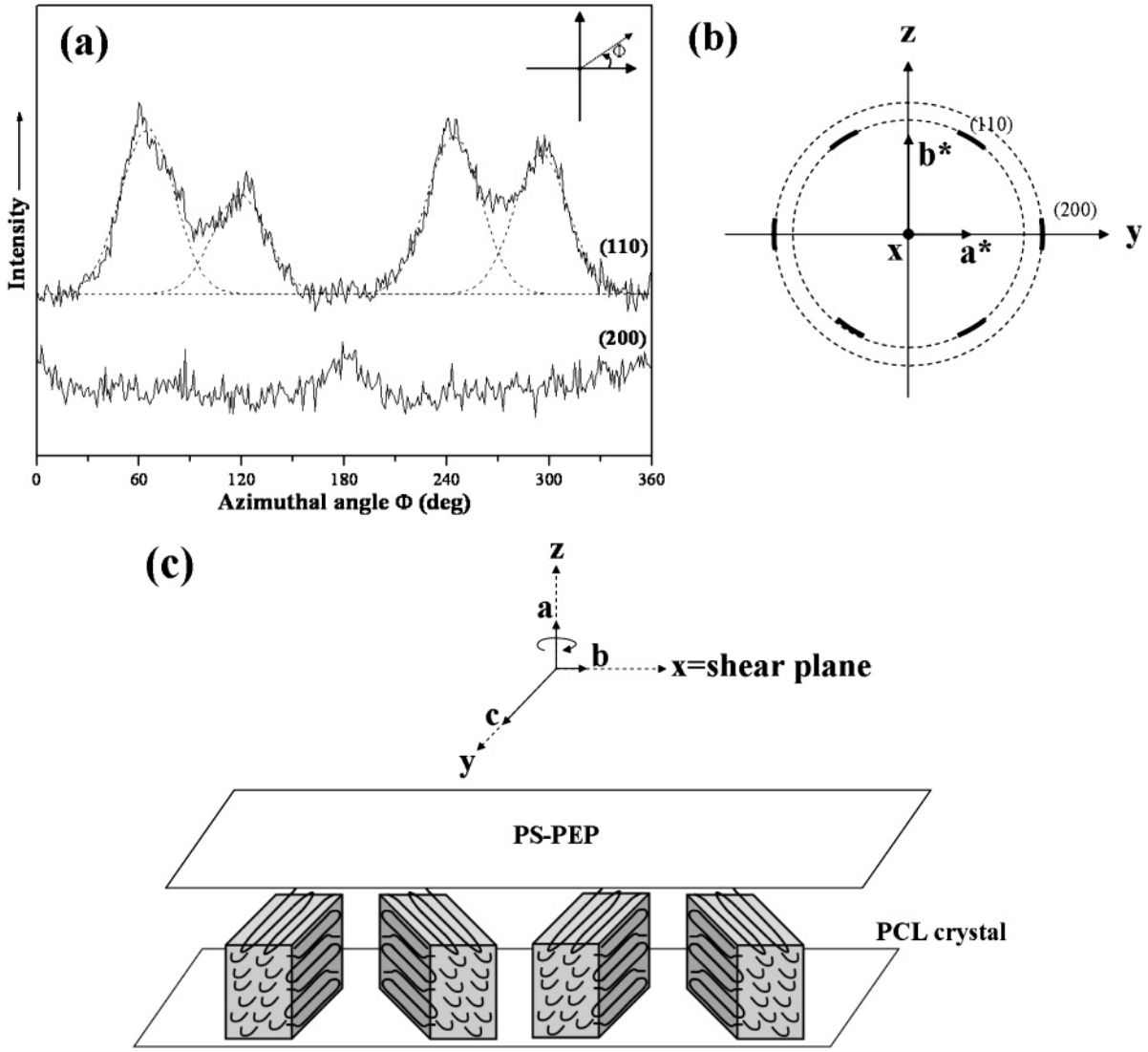

Figure 5. (a) Azimuthal scanning profiles of the {110} and {200} reflections of the WAXD patterns in Figure 3d for the PCL11/PS−PEP blends isothermally crystallized at 40 °C. (b) Schematic diagram of the WAXD pattern with indexed reflections. (c) Schematic diagram of the microstructure of oriented PCL11/PS−PEP samples isothermally crystallized at 40 °C from ordered melt at 100 °C. The crystallization of PCL is confined between the preformed lamellar PS layers, and *a* and *c* axes of the PCL crystals are preferentially parallel and perpendicular to the axes of the PS lamellar normal, respectively.

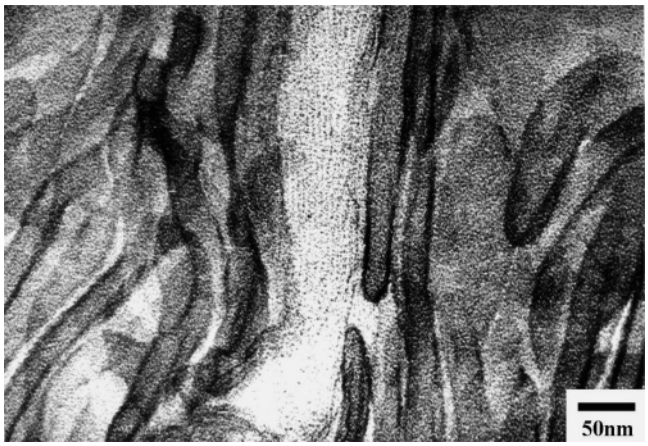

Figure 6. TEM micrograph of PCL3/PS−PEP blends. In the middle region of the TEM micrograph, alternate white and black thin stripes of PCL components are in between of PS−PEP component appeared as multilayer-like crystals.

Simultaneous Small-Angle X-ray Scattering (SAXS) and Wide-Angle X-ray Diffraction (WAXD). Simultaneous 2D SAXS and WAXD experiments were conducted at the synchrotron X-ray beamline X27C at the National Synchrotron Light Source (NSLS) in Brookhaven National Laboratory (BNL). The wavelength of the X-ray beam was 0.1366 nm. A MAR CCD X-ray detector (MAR) was used to collect the 2D SAXS patterns. A 1D linear profile was obtained by integration of the 2D pattern. The scattering angle of the SAXS pattern was calibrated using silver behenate, with the first-order scattering vector q^* ($q^* = 4\pi\lambda^{-1} \sin\theta$, where 2θ is the scattering angle) being 1.076 nm^{-1}. The diffraction peak positions and widths observed from WAXD experiments were carefully calibrated with silicon powder with 2θ being 28.4° under Cu Kα radiation. The azimuthal profiles for 2D WAXD patterns were obtained by scanning.

Transmission Electron Microscopy. The PCL/PS−PEP blends were cryo-microtomed at −120 °C for transmission electron microscopic (TEM) observations. A Reicher Ultracut microtome was equipped with a Reichert FCS cryochamber and a diamond knife. Staining was accomplished by exposing the samples to the vapor of a 4% aqueous RuO_4 solution for 30 min. Bright field TEM images of mass thickness contrast were obtained from the stained samples on a JEOL JEM-1200x transmission electron microscopy, at an accelerating voltage of 120 kV.

Differential Scanning Calorimetry (DSC). The samples were first heated to the maximum annealing temperature, T_{max}

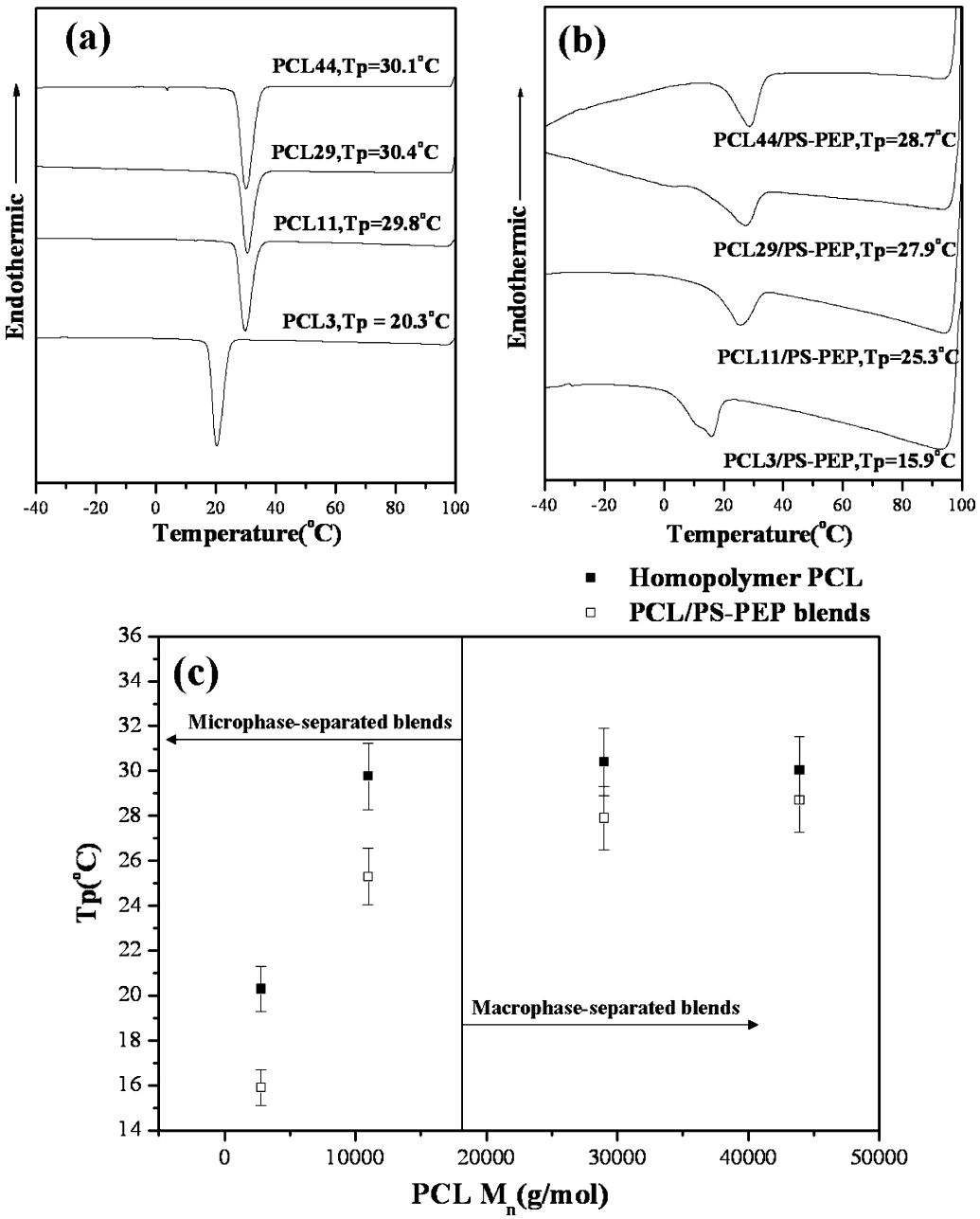

Figure 7. DSC thermograms of various (a) PCL homopolymers and (b) PCL/PS−PEP blends from the melt to −40 °C. The cooling rate is 10 °C/min for all the scans. (c) PCL molecular weight dependence of the peak temperature (T_p) in nonisothermal crystallization exotherm.

= 100 °C, for 3 min to eliminate the PCL crystalline residues formed during the preparation procedure using a Perkin-Elmer DSC7 equipped with an Intracooler. For nonisothermal crystallization experiments, the series of samples after melt mixing were first heated to T_{max} and then cooled to −50 °C at 10 °C/min. For isothermal crystallization experiments, the samples were first heated to T_{max} for 3 min and then rapidly cooled at 150 °C/min to preset temperature, T_c, for PCL crystallization. The melting temperature, T_m, and the heat of fusion, ΔH_m, of each sample were recorded by a scan rate of 10 °C/min in DSC. The melting temperature and endotherms at different heating rates were carefully calibrated using standard materials. The DSC sample weight was 6 mg in all treatments of DSC.

Results and Discussion

Physically Confined System. In our previous study,[36] two kinds of self-assembly morphology have been obtained by simply blending crystallizable PCL homopolymer with PS−PEP diblock copolymer via melt mixing. They are macrophase-separated and microphase-separated morphologies having PCL domain sizes above and below submicrometer, respectively. The microphase separation and the localization behavior of self-assembly PCL/PS−PEP blends system have been demonstrated in our previous works.[36] As shown (see Figure 1 in ref 36), microphase-separated lamellae were observed by TEM. There are no significant dispersed macrodomains observed in the blends containing low-molecular-weight PCL components (see Figures 1d−f in ref 36). Dispersed domains (bright area in picture) with submicron size were only obtained after the introduction of high-molecular-weight PCL components, as illustrated in Figure 1b,c in ref 36. The localized morphology was confirmed in terms of TEM observations by phase contrast imaging (see Figure 7b in ref 36). Without staining, the microdomains of the PS component appear

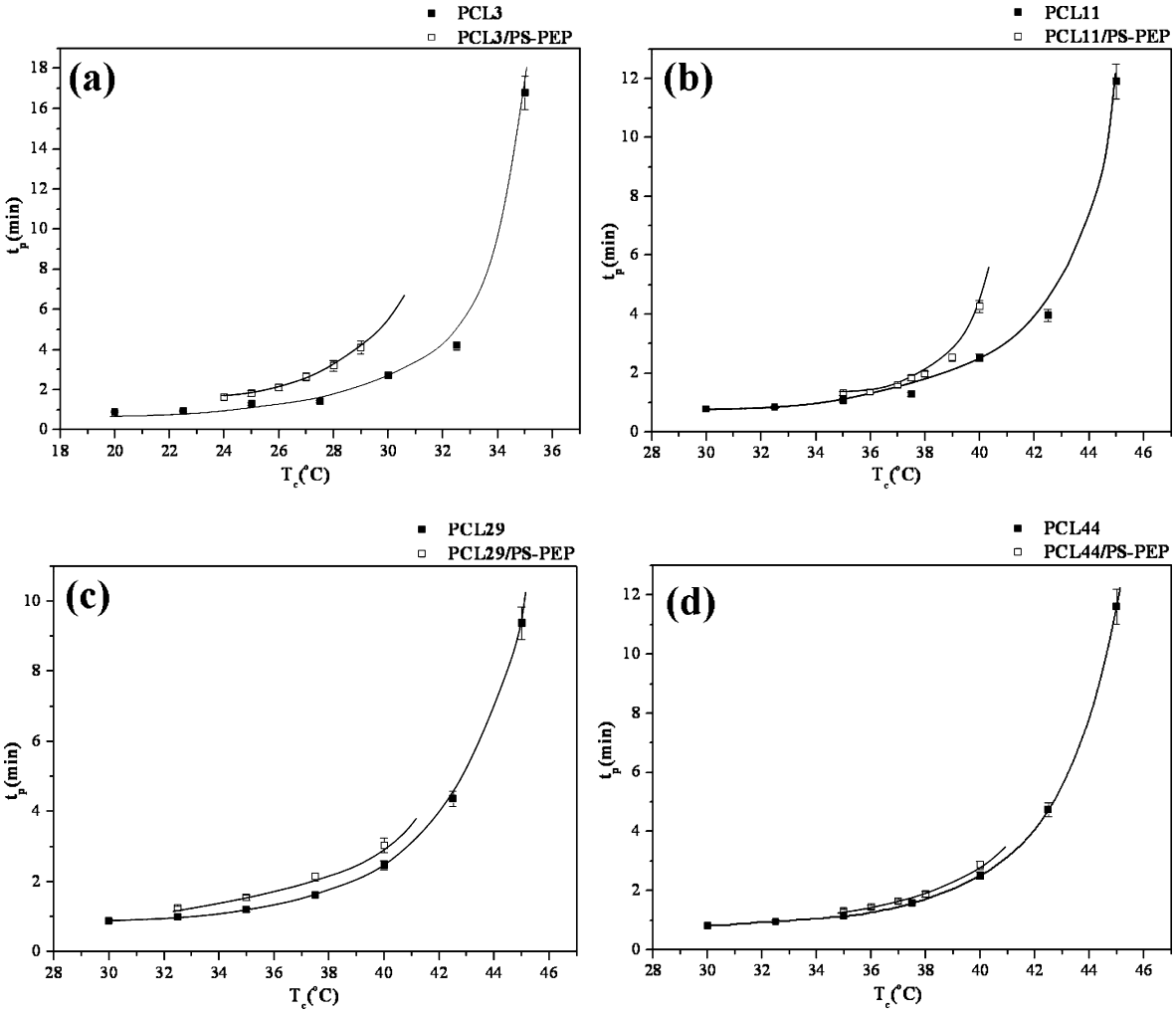

Figure 8. Crystallization temperature dependence of peak time of endothermic response (t_p) in isothermal crystallization of (a) PCL3/PS−PEP, (b) PCL11/PS−PEP, (c) PCL29/PS−PEP, and (d) PCL44/PS−PEP.

to be relatively dark under TEM by phase contrast at suitable underfocus owing to the effects of mean inner potential difference, whereas the microdomain of the PEP component appears light. Localized PCL microdomains can be identified due to the discernible contrast between the PS-rich and PCL-rich microdomains. Furthermore, from the 1D SAXS profiles, significant increase of d spacing for PCL/PS−PEP blends was observed in PCL/PS−PEP blends (Figures 2 and 6e in ref 36), suggesting PCL is truly localized and confined in the PS layers when PCL M_n is below 19 000 g/mol. Consistently, the DSC results of PCL/PS−PEP blends indicate that $T_{g,PS}$ decreases with decreasing of PCL molecular weight, but no significant change was obtained in $T_{g,PEP}$ even PCL M_n lower to 2800 g/mol.[36] As a result, the formation of microphase-separated lamellae is attributed to the effect of self-assembly for block copolymers in PCL/PS−PEP blends. The PCL component is of favor the PS block as compared to the PEP block because of the self-assembly-induced compatibility effect between PCL and PS so as to form localized PCL microdomains. By contrast, macrophase separation occurred in the blends of PS and PCL or PEP.

In summary, the occurrence of PCL macrophase separation from the PS−PEP matrix in melt-mixed PCL/PS−PEP blends was observed when the molecular weight of added PCL is fairly high (say above 19 000 g/mol). In contrast to the formation of macrophase separation, unique morphology having crystallizable PCL component localized in between the lamellar microdomains of PS−PEP was obtained when the molecular weight of added PCL is low. These unique morphologies give rise to a specific environment for crystallization under confinement (i.e., a physical confinement).

For neat PS−PEP, the order−disorder transition temperature has been identified to be above 300 °C.[38] Since the temperature for the occurrence of PCL crystallization is much smaller than the T_{ODT} of PS−PEP and the $T_{g,PS}$ of the PS-rich phase in blends is fairly higher than the T_c range of PCL, the PCL crystallization in the PCL/PS−PEP blends can be treated as crystallization under hard confinement. Different isothermally crystallized PCL samples in PCL/PS−PEP blends were then examined by TEM, and no significant change for phase-separated morphology after crystallization has been observed.

Crystallographic Orientation. Two-dimensional (2D) SAXS and WAXD experiments were carried out to study the PCL crystalline orientation relationship with respect to PS−PEP microstructure under confinement. For the concerns of shear-induced crystallization, we carried out the crystallization from the microphase-separated melt by simply annealing the samples above the melting temperature of PCL components before isothermal crystallization so that a confined environ-

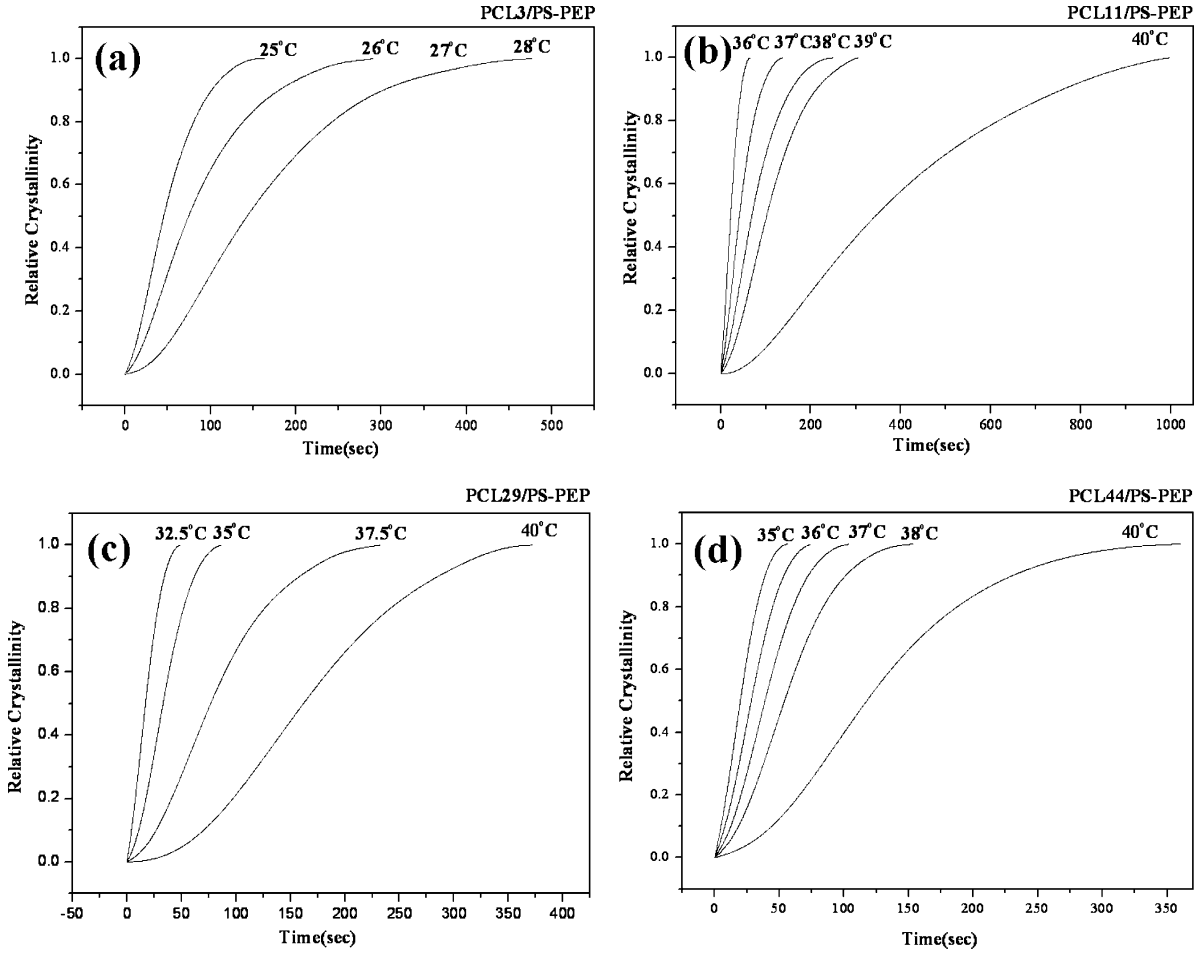

Figure 9. Crystallization time dependence of crystallinity for Avrami treatment at different crystallization temperatures of (a) PCL3/PS−PEP, (b) PCL11/PS−PEP, (c) PCL29/PS−PEP, and (d) PCL44/PS−PEP.

ment for melt crystallization was generated. Obviously, the appearance of oriented crystallization discussed below is due to the confinement effect instead of high shear force during mixing by Minimax. As a result, there is least consideration for the effect of shear-induced crystallization.

As shown in Figure 2, 2D SAXS patterns along *x*, *y,* and *z* direction indicate that oriented microphase-separated microdomains was obtained after melt-mixing for neat PS−PEP copolymer. Up to 4 orders of lamellar scattering peaks ($q/q^* = 1:2:3:4$) can be identified when the incident X-ray beams are along *x* and *y*, as shown in Figure 2a,b. By contrast, there is no significant scattering peak in the 2D SAXS pattern (Figure 2c). These SAXS results indicate that neat PS−PEP copolymer lamellae are aligned parallel to the *x*−*y* plane (i.e., shear plane). Similar to the neat PS−PEP, a series of PCL/PS−PEP blends can also be well aligned. For instance, the shear-aligned PCL11/PE-PEP samples were heated and then held at 100 °C for 3 min followed by quenching from melt to presetting temperature for isothermal crystallization. The oriented microphase-separated lamellar microstructure is preserved after PCL crystallization as evidenced by SAXS results (as illustrated in Figure 3a−c) so that the PCL is completely confined in the PS−PEP lamellar layer. For PCL crystallization at low crystallization temperature (for instance, at $T_c = -20$ °C), the 2D WAXD patterns exhibit typical ring pattern, suggesting that PCL crystals appear in random orientation under confinement.

By contrast, specific orientation of PCL crystals can be identified when the shear-aligned samples were crystallized at high crystallization temperature (for instance, 40 °C). The WAXD patterns along *x*, *y,* and *z* are shown in Figure 3d−f. 2D WAXD patterns along *x* and *y* directions are practically identical and exhibit an oriented feature. Only an isotropic ring pattern along *z* direction was observed (Figure 3f). Moreover, the 1D SAXS profile shows that *d* spacing of lamellar microstructure remains constant regardless of the evolution of crystallization, as illustrated in Figure 4, suggesting that the crystallization is truly carried out under confinement. On the basis of the orthorhombic lattice structure of PCL crystals with unit cell of $a = 0.749$ nm, $b = 0.498$ nm, $c = 1.703$ nm, and $\alpha = \beta = \gamma = 90°$,[39,40] the corresponding reflections were identified as {110} and {200} for orthorhombic crystalline structure. The azimuthal profiles of these reflections (Figure 5a) were obtained from the 2D WAXD pattern (Figure 3d). The intense {110} diffraction peaks are separated into four diffraction arcs and appear at $\Phi = 56°$, 124°, 236°, and 304°, and two {200} reflections appear at $\Phi = 0°$ and 180°. According to the azimuthal results, the diffraction pattern is illustrated in Figure 5b. The oriented diffractions along *a* axis suggest a parallel-type orientation having PCL crystalline chains parallel to the microphase-separated lamellae (i.e., the *x* and *y* directions).

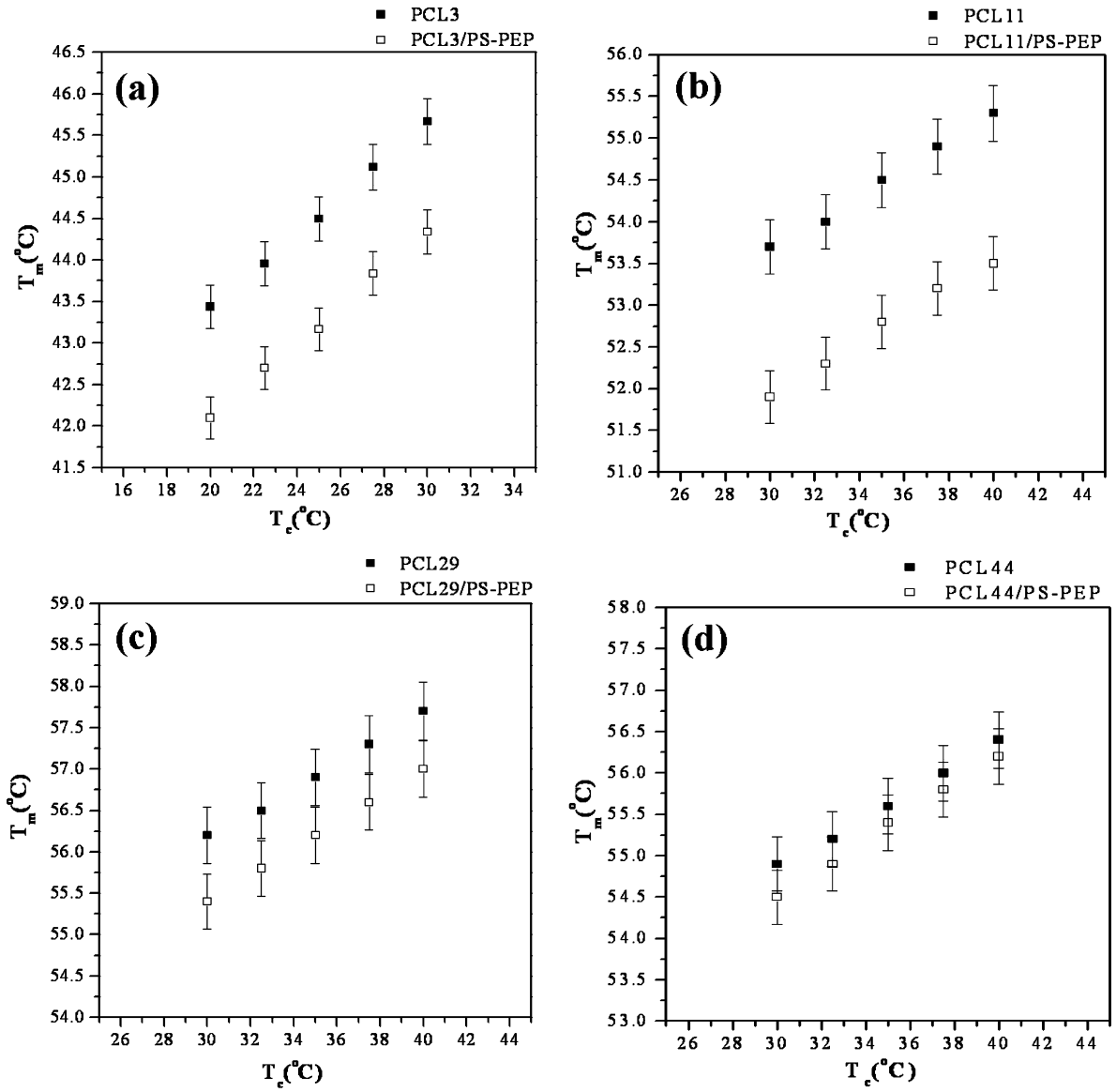

Figure 10. Crystallization temperature dependence of melting in (a) PCL3/PS−PEP, (b) PCL11/PS−PEP, (c) PCL29/PS−PEP, and (d) PCL44/PS−PEP.

Figure 5c shows the molecular disposition of crystalline PCL chains. Consequently, the crystalline orientation is strongly dependent upon the crystallization temperature.

Furthermore, the crystalline morphology of PCL in the PCL/PS−PEP blends after isothermal crystallization exhibits multilayer-like morphology, as illustrated in Figure 6. The PS microdomains appear relatively dark after preferentially staining by RuO_4, while the PEP microdomains appear relatively light. Contrary to amorphous parts of PCL that appear gray after staining, the crystalline parts of PCL exhibit significant contrast as bright regions due to the slow staining rate for dense PCL crystallites. As a result, the crystallization of PCL is indeed spatially confined within the vitrified layered structure, and the confined environment for crystallized PCL in microphase-separated morphology can be approximately regarded as one-dimensional confinement having confined size ranging from 50 to ca. 80 nm as determined by TEM and SAXS (see Figure 2 of ref 36).

Nonisothermal Crystallization. To study the effect of confinement on crystallization, the peak temperature of the nonisothermal crystallization exotherm, T_p, was obtained by a nonisothermal crystallization experiment during cooling. As illustrated in Figure 7a, the T_p of neat PCL homopolymer decreases with decreasing the molecular weight of PCL. The molecular weight dependence of the T_p of neat PCL homopolymers is, in principle, consistent with the results of previous studies.[41] The longer length of the crystalline chain requires larger undercooling to overcome the energy barrier of nucleation. Contrary to the T_p of neat PCL homopolymer, no significant change in T_p of PCL in the PCL44/PS−PEP blends has been found, whereas a slight decrease in T_p for PCL29/PS−PEP occurs, as shown in Figure 7b,c. As observed, both PCL29/PS−PEP and PCL44/PS−PEP blends appear to be macrophase-separated PCL domains with submicrometer size. However, the discrepancy between the T_p of neat PCL hompolymer and that of PCL in blends becomes significant once the self-assembly morphology appears as the behavior of PCL localization with the thickness of PCL microdomains below submicrometers. As a result, the effect of spatial confinement is insignificant due to the submicrometer size of macrophase separation, whereas the decrease in T_p becomes significant due to the

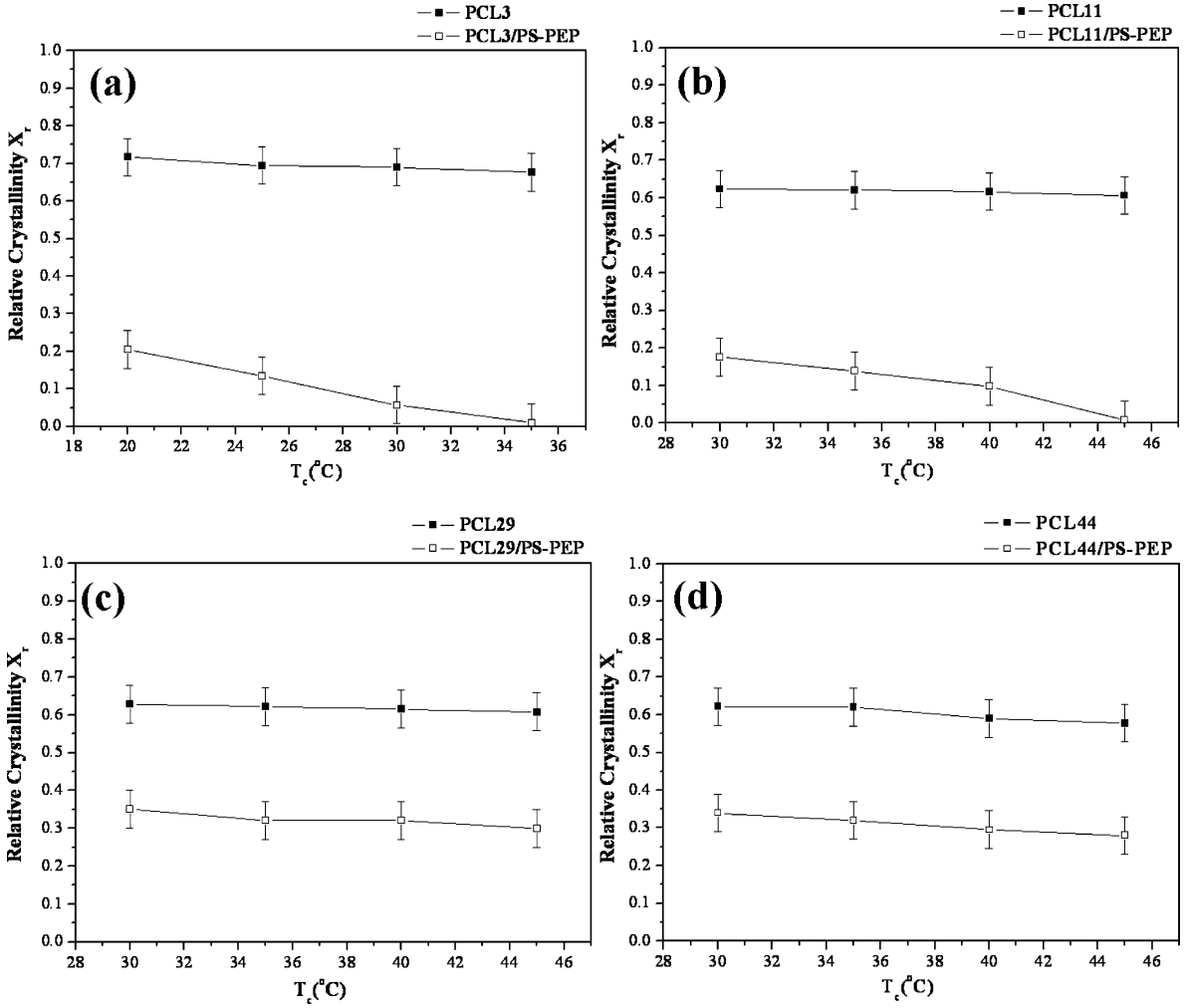

Figure 11. Crystallization temperature dependence of relative crystallinity (X_r) in isothermal crystallization of (a) PCL3/PS−PEP, (b) PCL11/PS−PEP, (c) PCL29/PS−PEP, and (d) PCL44/PS−PEP.

localization of PCL chains at which the confined size for PCL crystallization is below 100 nm. One explanation for the decrease in T_p might be attributed to the enhanced miscibility between PCL homopolymer and PS-rich blocks due to the effect of self-assembly for block copolymers as reported in our previous study. However, the change on miscibility is not profound as identified from our previous results of thermal analysis.[36]

Isothermal Crystallization Kinetics. To further examine the changes of crystallization rate and nucleation mechanism, isothermal crystallization for PCL in blends was carried out. The isothermal crystallization rate is expected to be approximately proportional to the reciprocal of the peak time of endothermic response, t_p, for isothermal crystallization. Figure 8 shows sets of the crystallization half-times at different crystallization temperatures for PCL crystallization. Similar to the results of nonisothermal crystallization, the decrease in crystallization rate as shown in Figure 8a,b is attributed to the effect of confinement, of which the confined size is below 100 nm. No significant change in crystallization rate (i.e., no significant confinement effect) was found when the crystallization of PCL was carried out in macrophase-separated blends (i.e., submicrometer size of PCL domains), as shown in Figure 8c,d.

Avrami treatment was carried out to examine the crystallization mechanism. According to $\ln(1 - X) = -Kt^n$, where X, K, and n are the fraction of crystallinity at time t, the prefactor, and Avrami index, respectively, crystallization kinetics can be analyzed in terms of the obtained n value. The results of the n values are listed in Table 1. The averaged value of n for the neat PCL crystallization is calculated as ca. 2.5, close to the predictive value, indicating a heterogeneous type of nucleation, in agreement with other studies.[42−44] The averaged value of n in confined systems, such as PCL3/PS−PEP and PCL11/PS−PEP blends, is 1.5, whereas the averaged value obtained in PCL29/PS−PEP and PCL44/PS−PEP blends is 1.8 (see below for reasons).

Table 1. Avrami Index of a Series of PCL Homopolymers and PCL/PS−PEP Blends

entry	Avrami exponent n (in average)	entry	Avrami exponent n (in average)
PCL3	2.5	PCL11/PS−PEP	1.5
PCL29	2.5	PCL29/PS−PEP	1.8
PCL44	2.5	PCL44/PS−PEP	1.8
PCL3/PS−PEP	1.5		

Register and co-workers explored the crystallization of the chemically confined system.[17,33] They found that the crystallization kinetics within the spherical confined shape exhibits homogeneous nucleation, of which the Avrami value is one and the crystallinity curve appears to be the first-order crystallization kinetics (i.e., exponential mode). By contrast, heterogeneous nucleation shows the traditional sigmoidal kinetics and has an

Avrami value large than one. Figure 9 shows the crystalline curves of crystallized PCL/PS−PEP blends; first-order kinetics was not obtained in all the blends. These results suggest that the crystallization of PCL in blends appears as a heterogeneous type of nucleation, and the crystallization kinetics is similar to that of homopolymer. Although the crystallization rate is affected by the confinement, the confined size in blends is not small enough to significantly change the crystallization mechanism. Consequently, the heterogeneous nucleation under confinement appears as typical values of Avrami indices below 2. We speculate that the confined effect on crystallization in physically confined system is similar to the effect in chemically confined system.

Melting Behavior. The melting behavior of PCL crystals in a confined environment is also different than that of the homopolymer. Figure 10 shows the melting points of PCL crystals in the PCL/PS−PEP blends and homopolymers with different molecular weights. As observed, blending of PCL and PS−PEP, in general, leads to the depression of melting. Contrary to the melting of homopolymers, the significant melting depression of PCL crystals can be recognized in blends having the behavior of localization for PCL (Figure 10a,b), whereas the phenomenon of melting depression is not noteworthy in macrophase-separated systems. By contrast, significant crystallinity depression was found in all the blends studied, as shown in Figure 11. The degree of relative crystallinity ($X_r = \Delta H_s/(w_{PCL}\Delta H_p)$) is defined as the ratio of the heat of fusion at the setting temperature (ΔH_s) to the heat of fusion of perfect crystalline PCL in the blends ($w_{PCL}\Delta H_p$), where w_{PCL} is the weight fraction of PCL in the blends. Nevertheless, the PCL crystallinity in microphase-separated blends (Figure 11a,b) appears to be a dramatic depression as compared to that of PCL homopolymers. By contrast, the change on relative crystallinity in macrophase-separated blends (Figure 11c,d) is not as significant as the change in microphase-separated blends. Furthermore, the change on the relative crystallinity is strongly dependent upon crystallization temperatures, suggesting that the confinement effect on crystallinity becomes much profound in microphase-separated blends, particularly crystallized at higher temperature.

Conclusion

Obviously, the changes of crystallization and melting behavior are truly correlated with the confinement effect. Macrophase-separated and microphase-separated morphology were obtained in the self-assembly PCL/PS−PEP blends so as to create one-dimensional confined environments (i.e., lamellar confinement) having various confined sizes. In macrophase-separated blends, the confined effects on crystallization and melting are not significant. By contrast, noteworthy changes on crystallization rate and melting can be recognized in microphase-separated blends. The discrepancies in PCL crystallization behavior between macrophase-separated and microphase-separated morphologies are attributed to the size effect on confinement. The effective confinement is attributed to the localization behavior of PCL chains at which the one-dimensional confined size is below submicrometer.

Acknowledgment. The financial support of the National Science Council (Grant NSC 89-2216-E-005-023) is acknowledged. We thank Dr. B. S. Hsiao of the Chemistry Department, State University of New York at Stony Brook, and Drs. S. Ran, I. Sics, and C. A. Avila-Orta of the National Synchrotron Light Source at Brookhaven National Laboratory and Dr. Y.-S. Sun of the National Synchrotron Radiation Research Center for their help in Synchrotron SAXS experiments. R.M.H. also thanks Dr. S. Z. D. Cheng of Institute of Polymer Science of University of Akron for his helpful discussion. Our appreciation is extended to Ms. P.-C. Chao of Regional Instruments Center at NCHU for their help in TEM experiments.

References and Notes

(1) Whitesides, G. M.; Grzybowski, B. *Science* **2002**, *295*, 2418.
(2) Nojima, S.; Kato, K.; Yamamoto, S.; Ashida, T. *Macromolecules* **1992**, *25*, 2237.
(3) Ryan, A. J.; Hamley, I. W.; Bras, W.; Bates, F. S. *Macromolecules* **1995**, *28*, 3860.
(4) Yang, Y.-W.; Tanodekaew, S.; Mai, S.-M.; Booth, C.; Ryan, A. J.; Bras, W.; Viras, K. *Macromolecules* **1995**, *28*, 6029.
(5) Zhu, L.; Chen, Y.; Zhang, A.; Calhoun, B. H.; Chun, M.; Quirk, R. P.; Cheng, S. Z. D.; Hsiao, B. S.; Yeh, F.; Hashimoto, T. *Phys. Rev. B* **1999**, *60*, 10022.
(6) Cohen, R. E.; Cheng, P. L.; Douzinas, K.; Kofinas, P.; Berney, C. V. *Macromolecules* **1990**, *23*, 324.
(7) Douzinas, K. C.; Cohen, R. E. *Macromolecules* **1992**, *25*, 5030.
(8) Cohen, R. E.; Bellare, A.; Drzewinski, M. A. *Macromolecules* **1994**, *27*, 2321.
(9) Khandpur, A. K.; Macosko, C. W.; Bates, F. S. *J. Polym. Sci., Part B: Polym. Phys.* **1995**, *33*, 247.
(10) Liu, L.-Z.; Yeh, F.; Chu, B. *Macromolecules* **1996**, *29*, 5336.
(11) Hamley, I. W.; Fairclough, J. P. A.; Terrill, N. J.; Ryan, A. J.; Lipic, P. M.; Bates, F. S.; Towns-Andrews, E. *Macromolecules* **1996**, *29*, 8835.
(12) Hamley, I. W.; Fairclough, J. P. A.; Ryan, A. J.; Bates, F. S.; Towns-Andrews, E. *Polymer* **1996**, *37,* 4425.
(13) Quiram, D. J.; Register, R. A.; Marchand, G. R.; Adamson, D. H. *Macromolecules* **1998**, *31*, 4891.
(14) Hamley, I. W.; Fairclough, J. P. A.; Bates, F. S.; Ryan, A. J. *Polymer* **1998**, *39*, 1429.
(15) Weimann, P. A.; Hajduk, D. A.; Chu, C.; Chaffin, K. A.; Brodil, J. C.; Bates, F. S. *J. Polym. Sci., Part B: Polym. Phys.* **1999**, *37*, 2053.
(16) Zhu, L.; Cheng, S. Z. D.; Calhoun, B. H.; Ge, G.; Quirk, R. P.; Thomas, E. L.; Hsiao, B. S.; Yeh, F.; Lotz, B. *J. Am. Chem. Soc.* **2000**, *122*, 5957.
(17) Loo, Y. L.; Register, R. A.; Ryan, A. J. *Phys. Rev. Lett.* **2000**, *84*, 4120.
(18) Zhu, L.; Cheng, S. Z. D.; Calhoun, B. H.; Ge, Q.; Quirk, R. P.; Thomas, E. L.; Hsiao, B. S.; Yeh, F.; Lotz, B. *Polymer* **2001**, *42*, 5829.
(19) Zhu, L.; Calhoun, B. H.; Ge, Q.; Quirk, R. P.; Cheng, S. Z. D.; Thomas, E. L.; Hsiao, B. S.; Yeh, F.; Liu, L.; Lotz, B. *Macromolecules* **2001**, *34*, 1244.
(20) Sun, L.; Zhu, L.; Ge, Q.; Quirk, R. P.; Xue, C. C.; Cheng, S. Z. D.; Hsiao, B. S.; Avila-Orta, C. A.; Sics, I.; Cantino, M. E. *Polymer* **2004**, *45*, 2931.
(21) Huang, P.; Zhu, L.; Guo, Y.; Ge, Q.; Jing, A. J.; Chen, W. Y.; Quirk, R. P.; Cheng, S. Z. D.; Thomas, E. L.; Lotz, B.; Hsiao, B. S.; Avila-Orta, C. A.; Sics, I. *Macromolecules* **2004**, *37*, 3689.
(22) Ho, R.-M.; Chung, T.-M.; Tsai, J.-C.; Kuo, J.-C.; Hsiao, B. S.; Sics, I. *Macromol. Rapid Commun.* **2005**, *26*, 10.
(23) Ishikawa, S.; Ishizu, K.; Fukutomi, T. *Eur. Polym. J.* **1992**, *28*, 1219.
(24) Kofinas, P.; Cohen, R. E. *Macromolecules* **1994**, *27*, 3002.
(25) Quiram, D. J.; Register, R. A.; Marchand, G. R. *Macromolecules* **1997**, *30*, 4551.
(26) Mai, S.-M.; Fairclough, J. P. A.; Viras, K.; Gorry, P. A.; Hamley, I. W.; Ryan, A. J.; Booth, C. *Macromolecules* **1997**, *30*, 8392.
(27) Hillmyer, M. A.; Bates, F. S. *Macromol. Symp.* **1997**, *117*, 121.
(28) Chen, H.-L.; Hsiao, S. C.; Lin, T. L.; Yamauchi, K.; Hasegawa, H.; Hashimoto, T. *Macromolecules* **2001**, *34*, 671.

(29) Chen, H.-L.; Wu, J. C.; Lin, T.-L.; Lin, J. S. *Macromolecules* **2001**, *34*, 6936.
(30) Loo, Y.-L.; Register, R. A.; Ryan, A. J.; Dee, G. T. *Macromolecules* **2001**, *34*, 8968.
(31) Xu, J.-T.; Turner, S. C.; Fairclough, J. P. A.; Mai, S.-M.; Ryan, A. J.; Chaibundit, C.; Booth, C. *Macromolecules* **2002**, *35*, 3614.
(32) Xu, J.-T.; Fairclough, J. P. A.; Mai, S.-M.; Ryan, A. J.; Chaibundit, C. *Macromolecules* **2002**, *35*, 6937.
(33) Loo, Y.-L.; Register, R. A.; Ryan, A. J. *Macromolecules* **2002**, *35*, 2365.
(34) Ho, R.-M.; Lin, F.-H.; Tsai, C.-C.; Lin, C.-C.; Ko, B.-T.; Hsiao, B. S.; Sics, I. *Macromolecules* **2004**, *37*, 5985.
(35) Bates, F. S.; Fredrickson, G. H. *Annu. Rev. Phys. Chem.* **1990**, *41*, 525.
(36) Ho, R.-M.; Chiang, Y.-W.; Lin, C.-C.; Bai, S.-J. *Macromolecules* **2002**, *35*, 1299.
(37) Ko, B.-T.; Lin, C.-C. *Macromolecules* **1999**, *32*, 8296.
(38) Han, C. D.; Choi, S.; Lee, K. M.; Hahn, S. F. *Macromolecules* **2004**, *37*, 7290.
(39) Chatani, Y.; Tadokoro, H.; Yamashita, Y. *Polym. J.* **1970**, *1*, 555.
(40) Tian, D.; Halleux, O.; Dubois, P.; Jerome, R. *Macromolecules* **1998**, *31*, 924.
(41) Albuerne, J.; Marquez, L.; Muller, A. J.; Raquez, J. M.; Degee, Ph.; Dubois, Ph.; Castelletto, V.; Hamley, I. W. *Macromolecules* **2003**, *36*, 1633.
(42) Goulet, L.; Pudhomme, R. E. *J. Polym. Sci., Polym. Phys.* **1990**, *28*, 2329.
(43) Skoglund, P.; Fransson, A. *J. Appl. Polym. Sci.* **1996**, *61*, 2455.
(44) Balsamo, V.; Calzadilla, N.; Mora, G. A.; Müller, J. *J. Polym. Sci., Polym. Phys.* **2001**, *39*, 771.

MA047515L